Strength of flexible composites: Damage tolerance in compliant unidirectional fiber reinforced composites

W. M. Peterson[1]
Montana State University, Bozeman, Montana, 59717

N. M. Hossain[2]
Eastern Washington University, Cheney, WA, 99004

K. Woo[3]
Chungbuk National University, Cheongju, Chungbuk 361-763, Republic of Korea

and

C. H. Jenkins[4]
Montana State University, Bozeman, Montana, 59717

The strength of advanced materials and thin-film membranes for gossamer spacecraft may be enhanced by small-diameter fiber reinforcements, where the resulting composite material offers improved damage resistance and greater space environment survivability while maintaining flexibility and low mass. One of the potential advantages of decreasing the fiber diameter in fiber-reinforced composites is the resulting increase of surface area at the fiber-matrix interface, which, for example, may help to compensate for broken fibers and imperfect fiber-matrix bonding. In this paper, the load redistribution from broken fibers to unbroken neighboring fibers in a flexible matrix is investigated using 3D finite element (FE) micromechanical models under longitudinal tensile loading. The fiber load transfer characteristic length (L_c), also known as the ineffective fiber length, of a composite with reduced fiber diameter (RFC) is compared to that of a conventional fiber-diameter composite (CFC) with the same fiber volume fraction. The work presented here also compares fiber diameter scaling effects upon the initiation and evolution of fiber-matrix interfacial damage using a cohesive element fracture mechanics method. Results suggest that for a constant fiber volume fraction, as the fiber diameter is reduced both L_c and the maximum interfacial shear stress decrease in the damage models, while damage tolerance is increased.

Nomenclature

A	=	cross sectional area of fiber
A_s	=	surface area of fiber
CFC	=	conventional fiber-diameter composite
CZM	=	cohesive zone model
D, d	=	fiber diameter (CFC, RFC)
L	=	length of unit cell
L_c	=	fiber load transfer characteristic length
N, n	=	number of fibers in unit cell (CFC, RFC)
RBC	=	repeating boundary condition

[1] Graduate Student, Department of Mechanical and Industrial Engineering. Student Member AIAA.
[2] Assistant Professor, Department of Engineering and Design. Member AIAA.
[3] Professor, Department of Structural System and CAE. Member AIAA.
[4] Professor and Head, Department of Mechanical and Industrial Engineering. Associate Fellow AIAA.

RF = reaction force (absolute value)
RFC = reduced fiber-diameter composite
RVE = representative volume element
R, r = fiber radius (CFC, RFC)
UC = unit cell
u, δ = displacement
ur = rotation
V_f = fiber volume fraction
W = side dimension of unit cell
z_c = 90% stress transfer fiber length
σ = axial stress in fiber
τ = shear stress at fiber-matrix interface

I. Introduction

MATERIALS and technologies developed for use in space-based gossamer structures must satisfy a challenging set of requirements. Desirable materials must possess qualities that include ultra-low mass and high flexibility in order to achieve lightweight and compact launch characteristics, while simultaneously retaining an ability to perform with a high level of reliability over the life of the spacecraft. Advancements in deployment and rigidization technologies must enable the metamorphosis of small launch packages into large, stable, and often complicated space-based configurations. The benefits resulting from satisfying these demanding requirements are quite great. The successful development of gossamer spacecraft technologies holds the promise of reducing costs associated with space missions, and may provide the means for the construction of much larger space-based structures than are currently possible[1].

The combination of ultra-low mass, high flexibility, durability, and longevity requirements often cannot be fulfilled by conventional materials. Typically, commercially available thin-film polyesters and polyimides have been used in a number of space missions and prototype gossamer structures. However, previous studies have shown that many of these polymers suffer from significant degradation in low earth orbit (LEO), exposure to solar radiation, thermal cycling, and micrometerioid impact. In order to address these issues, improved polymeric materials and new materials with combinations of desirable properties are being developed. For example, composites lend themselves easily as rigidizable structural materials, which are initially flexible but become rigid when exposed to an external influence such as heat, cold, or UV radiation. In the case of inflatable structures and for gossamer sails, flexible membranes may be reinforced with long, thin fibers. There are certain advantages in reducing the reinforcing fiber diameter compared to conventional fibers. Among the advantages important to gossamer spacecraft are increased flexibility and more compact stowage since bend radius scales with fiber diameter. Moreover, given that the thickness of many gossamer membranes may be considerably less than conventional fiber diameters, going to smaller diameter fibers may be the only practical solution.

A substantial amount of research into the mechanical behavior of composite materials has been performed in recent decades. In micromechanical approaches such as those documented by Aboudi,[2,3] the overall behavior of periodic multiphase composite materials is explored through the consideration of the response of the individual constituents, their volume fractions, and the detailed interaction between the phases in a representative volume element (RVE). Models for the elastic analysis of stress transfer between the fiber and the matrix in a composite material were developed by Cox[4] and by Nairn.[5] Goh et al.[6] compared solutions for different shear-lag models. Chon et al.[7] developed an analytical solution for predicting the axial and interfacial shear stress distributions along a single fiber of a randomly oriented chopped-fiber composite. Xia et al.[8] and Li et al.[9] compared shear-lag theories with finite element (FE) models for stress transfer in a fiber-reinforced composite. Milliren[10] compared the stress distributions from various FE meshes, geometries, and boundary conditions with standard shear-lag theories. Hossain et al.[11] studied the effect of fiber diameter on composite strength by developing several unit cell models with reduced fiber diameter while keeping the fiber volume fraction the same.

The shear-lag concept for composite materials has developed into a common analysis method used to examine stress transfer between a matrix and a fiber reinforcing phase. Shear-lag models are often represented by a single fiber embedded within a matrix, whereby loads are transmitted from the matrix to the fiber, typically in an arrangement of concentric cylinders. This configuration is valuable for its ability to represent broken fibers within a composite material, and to determine the length required for the broken fiber to recover its load carrying capacity.[8] This recovery length of fiber is generally referred to as the ineffective fiber length, or the length of fiber required before 90% of the maximum fiber stress has developed. Shear-lag models of various levels of complexity are found

in the literature, ranging from the relatively simple linear elastic to those which incorporate material viscoelasticity, strain hardening, and damage parameters in an effort to reproduce experimental data. In most models, it appears that analytical shear-lag methods accurately predict fiber axial stresses, but have lower accuracy when predicting the shear stress at the fiber-matrix interface.[5] To overcome this, detailed finite element models have been utilized.[8,9]

Additionally, the cohesive zone model (CZM) has become an important computational tool for simulating the progressive damage and failure of materials. The cohesive zone approach, first proposed by Barenblatt[12] and Dugdale,[13] is typically expressed in terms of cohesive forces, or tractions, in relation to separation distances within a small fracture process zone in front of the crack tip. CZMs have been successfully used to model a number of fracture and failure processes, most notably in the analysis of interfacial delamination such as between the plies of a composite layup. Many alternative formulations of CZMs based on the Barenblatt and Dugdale models have been developed, such as the polynomial and exponential types of traction-separation relations of Needleman,[14] the trapezoidal type of Tvergaard and Hutchinson,[15] and the quadratic type with mode-mixity of Camanho and Davila.[16] Chandra et al.[17] detailed the importance of the shape of the traction-separation relation in addition to two independent parameters – the cohesive energy, and either the cohesive strength or the critical separation displacement – in order to accurately simulate the macroscopic mechanical behavior of composites.

This paper and its companion[18] compares the effects of reducing the fiber diameter on load transfer and stress distributions at broken fibers embedded in a flexible matrix using finite element micromechanical models. In this work, the fiber characteristic load transfer length (L_c) (also known as the ineffective fiber length) of a composite with reduced fiber diameter (RFC) is compared to that of a conventional fiber-diameter composite (CFC) with the same fiber volume fraction. In the CFC the fiber diameter $D = 14$ μm is used, while in the the RFC the fiber diameter used is $d = 7$ μm. The work presented here also compares fiber diameter scaling effects upon the initiation and evolution of fiber-matrix interfacial damage using a cohesive element fracture mechanics method. Reductions in the fiber load transfer characteristic length and the magnitude of the shear and axial stresses developed in these models are used as performance indicators.

II. Motivation for Flexible Composites with Reduced Fiber Diameters

In response to the need for advanced materials for gossamer spacecraft, composites may be designed which offer improved tear and damage resistance, and greater space environment survivability while maintaining flexibility and low mass.

A. Fiber Diameter and Fiber-Matrix Interface Surface Area

In many high performance composites the reinforcing phase is composed of long, thin fibers of high stiffness while the matrix generally has relatively low mechanical properties. In the common engineering terminology, a composite material is a structural combination of two or more constituent materials. Generally, one constituent is used as a stiff reinforcing phase which is embedded within a tough matrix phase. The matrix phase exists to bind the reinforcement phase together and provide a medium in which to distribute loads between the reinforcements. The resulting composite material exhibits properties unique to the particular combination of the constituents. In certain applications, composites offer advantages over conventional homogenous materials, which often include improvements in stiffness, strength, fatigue resistance, and thermal conductivity while reducing mass.

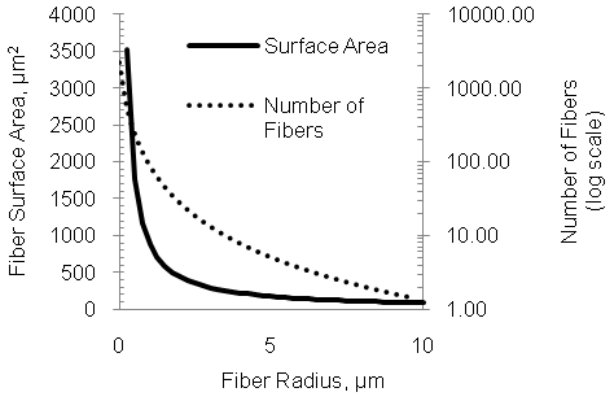

Figure 1. Fiber-matrix interfacial surface area as a function of radius. *Results shown for a constant fiber volume fraction of $V_f = 0.3$.*

As illustrated in Fig. 1, reducing the fiber diameter while maintaining a constant fiber volume fraction increases the surface area A_s at the fiber-matrix interface.[11] Furthermore, as shown in Eqs. (1) through (3), if N conventional fibers of diameter D are replaced by n smaller fibers of diameter d while V_f remains constant, the surface area increases by a factor of $(n/N)^{1/2}$.

$$A_{s,CFC} = N\pi DL \qquad \text{and} \qquad A_{s,RFC} = n\pi dL \tag{1}$$

From Eqs. (1) the diameter d is found to be

$$d = D\sqrt{N/n} \tag{2}$$

Then the reduced fiber diameter composite surface area, $A_{s,RFC}$ becomes

$$A_{s,RFC} = n\pi DL\sqrt{N/n} = \frac{n}{N}\sqrt{\frac{N}{n}}A_{s,CFC} \tag{3a}$$

$$A_{s,RFC} = A_{s,CFC}\sqrt{n/N} \tag{3b}$$

B. Fiber Diameter and Bending Stiffness

The flexibility for a given fiber material is enhanced by decreasing the diameter d, and can be shown to be inversely proportional to the fourth power of the fiber diameter.[19] For example, consider the differential form of the linear elastic strain energy of a cantilever beam in bending

$$U = \int_0^L \frac{EI}{2}\left(\frac{d^2v}{dx^2}\right)^2 dx = \frac{P^2L^3}{6EI} = \frac{1}{2}P\delta = W \tag{4}$$

where E is the elastic modulus of the material, P is the loading force, L is the beam length, δ is the tip displacement, and I is the second area moment of inertia for a cylindrical beam. For the linear elastic case the strain energy, U, equals the work done in bending, W. From Eq. (4) the beam stiffness is found to be

$$k = 3EI/L^3 \tag{5}$$

Thus, the flexibility of a fiber for a specified material is inversely proportional to d^4, and decreasing the diameter increases flexibility.

$$Flexibility = \frac{1}{k} \propto \frac{1}{EI} \propto \frac{1}{d^4} \tag{6}$$

III. Micromechanical Finite Element Models

Several 3D finite element (FE) models were used to the micromechanical behavior of a broken fiber embedded within a matrix. In this research the finite element code Abaqus was used to build, analyze, and obtain results from each unit cell (UC) model as described below.

A. The Representative Volume Element

Composites are intrinsically complex structures. In order to conserve computational resources, various idealizations are commonly used in order to represent the fundamental microstructure of a composite. For example, a representative volume element (RVE) is generally defined as a sufficiently large volume of a heterogeneous material that may be used to capture a statistical sampling of any essential features.[20] Such features include the matrix and fibers as well as fiber breaks, voids, matrix cracks, etc. Typical RVEs are still quite large and computationally intensive. Smaller RVEs may be obtained when certain assumptions are made about the statistical occurrence of fibers, flaws (such as the voids seen in Fig. 2), the geometric arrangement of features, and how they may vary

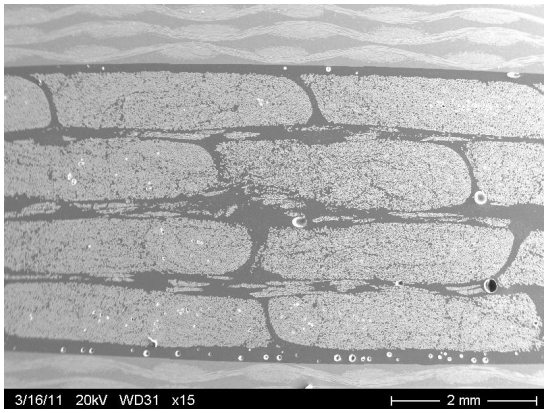

Figure 2. Cross section of typical $[45/45]_S$ glass/epoxy laminate. *SEM, Magnification x15.*

across the region of interest. When assuming that a composite exhibits a large degree of periodicity and a regular occurrence of features, smaller RVEs may be substituted and may be termed unit cells (UC). Often, a UC assumes a regular fiber distribution in either a hexagonal or square packing arrangement, which facilitates the application of repeating boundary conditions in order to represent the global composite (such RBCs, in fact, represent an infinitely repeating plane of unit cells). The scanning electron microscope images (SEM), courtesy of the Montana State University Mechanical and Industrial Engineering Dept., seen in Figs. 2 through 4 show a cross section of a typical unidirectional glass/epoxy composite laminate. Fig. 2 first illustrates the arrangement of fiber bundles (and several voids) in a laminate cross-section; in Fig. 3 both the individual strands and fiber bundles are apparent at an intermediate magnification; and in Fig. 4 the arrangement of individual fiber strands within a fiber bundle are shown.

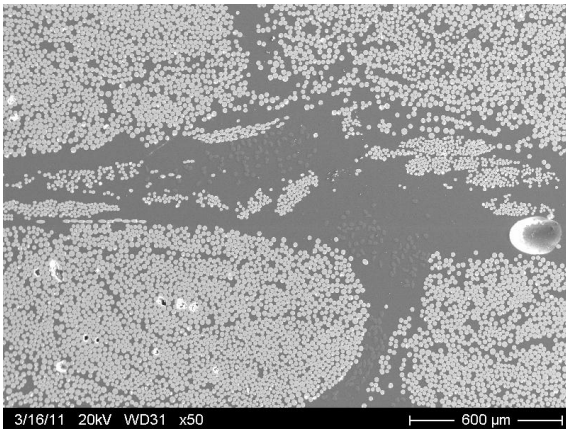

Figure 3. Cross section of typical $[45/45]_S$ glass/epoxy laminate. *SEM, Magnification x50.*

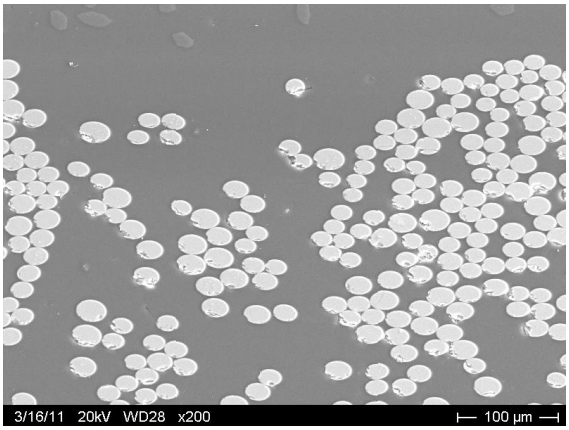

Figure 4. Unidirectional e-glass fibers in Hexion resin epoxy. *SEM, Magnification x200.*

B. Infinitely Repeating Unit Cell

In the work presented here, the unit cell representation of a composite has been utilized. A square packing arrangement of fibers has been assumed, which allows for a straightforward placement of repeating boundary conditions (RBCs). Through the use of symmetry and RBCs, the development of unit cells used for CFC and RFC models is shown in Fig. 5. When comparisons are made between fiber diameters, the models developed here assume the same fiber volume fraction occurs in both CFC and RFC, where $V_{f,CFC} = V_{f,RFC}$. This requires the total *fiber* cross-sectional area remains constant in both CFC and RFC unit cells, and the total length of each unit cell is also identical. Note that due to the symmetry of the unit cell models and the assumption that fibers are arranged in a square array, only a one-quarter representation of a single fiber is required in this finite element model. The quarter-symmetric single fiber unit cell with repeating boundary conditions is illustrated in Fig. 6.

The following symmetry and boundary conditions have been placed on the quarter-symmetric unit cell FE models, representing an infinitely repeating plane of fibers arranged in a square array, with a tensile load placed on the matrix surface in the fiber axial direction. These boundary conditions have been chosen in order to remain consistent with shear-lag theory. The notation *u* indicates displacent and *ur* is rotation with respect to the global *1, 2, 3* axes. Symmetry boundary conditions are applied to the left and bottom surfaces:

1) $u_1(0, y, z) = ur_2 = ur_3 = 0$
2) $u_2(x, W, z) = ur_1 = ur_3 = 0$

The rear surface at $z = 0$ is constrained in the *z*-direction:

3) $u_3(x, y, 0) = 0$

Repeating boundary conditions are applied to the top and right surfaces of the model:

4) $u_1(W, y, z) = \delta_1$
5) $u_2(x, W, z) = \delta_2$

Notice that the RBCs are such that all nodes on the right surface displace the same amount in the *x*-direction, and similarly, all nodes on the top surface displace the same amount in the *y*-direction. Thus, each surface remains planar. This is the most direct method to apply a repeating boundary condition on a unit cell, and is common in the literature.

The tensile boundary displacement is applied to the matrix material at the front surface, in the fiber axial direction:

6) $u_3(x, y, L) = \delta_{applied}$

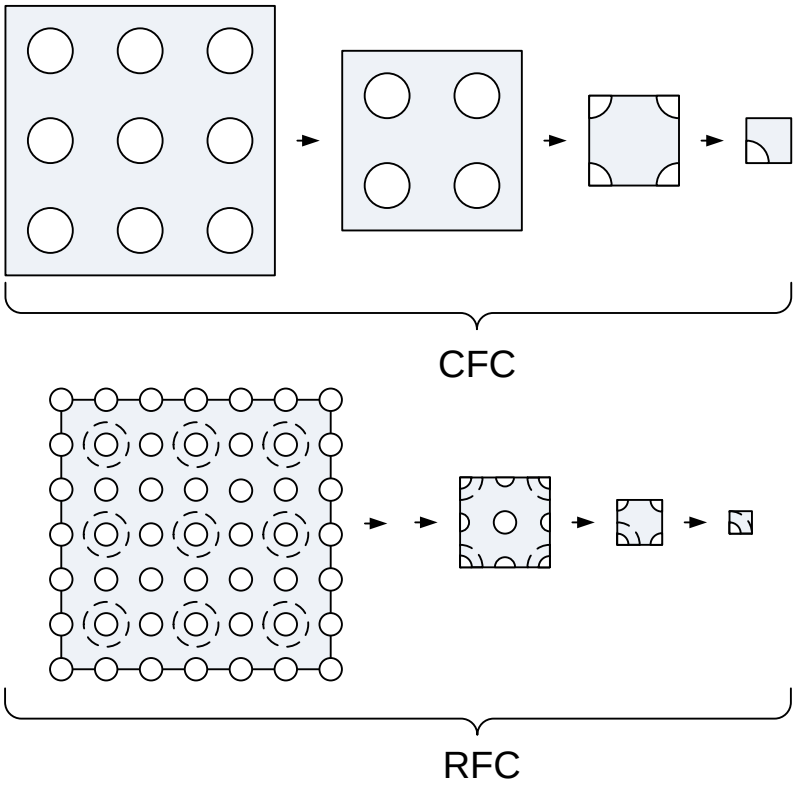

Figure 5. Assumed square arrangement of fibers and the development of the final unit cell for CFC and RFC. *Dotted lines in the RFC unit cell indicate where CFC fibers would be located for the same total V_f. Also, note that in this arrangement, every fiber is assumed to be broken in the same plane. All loading is performed in the shaded matrix region.*

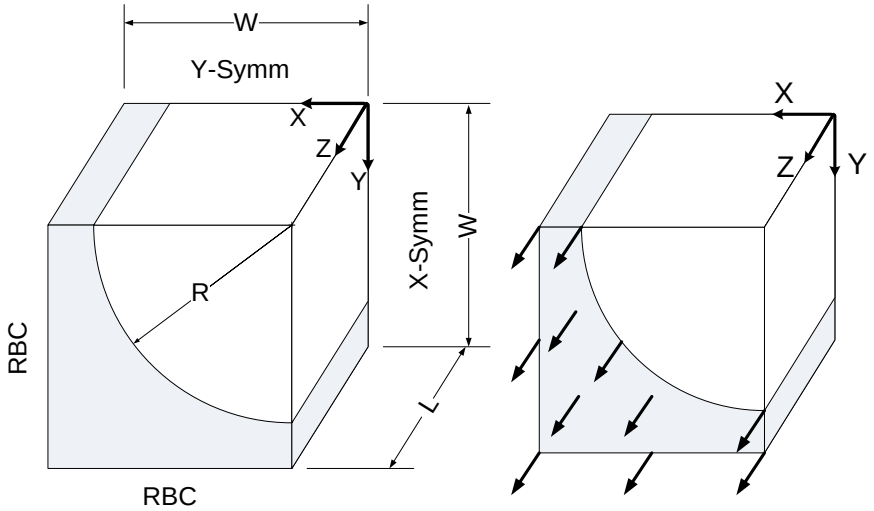

Figure 6. Unit cell with a single fiber. *Fiber is assumed broken. All loading is performed on the shaded matrix region only. Note the model is shown rotated in order to show the fiber more clearly.*

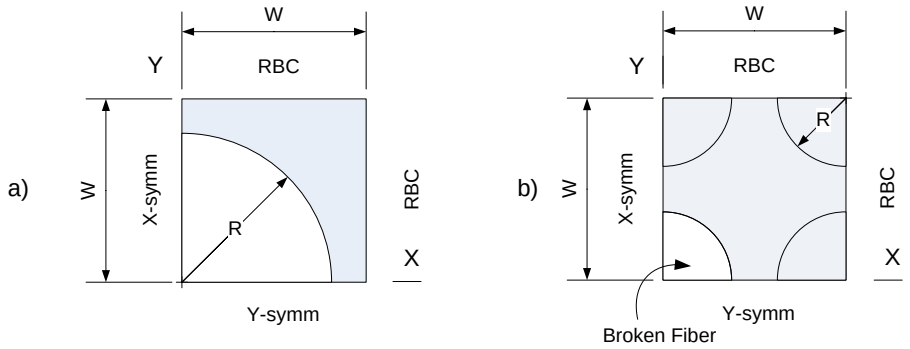

Figure 7. (a) Fully damaged unit cell with a single fiber, and (b) Partially damaged unit cell with four fibers. *All loading is performed in the shaded regions only.*

C. Infinitely Repeating Unit Cell with Partial Initial Damage

Analyses were also performed on a reduced fiber-diameter unit cell in which only one out of nine (1:9) fibers were broken. These RFC unit cells with partial initial damage were developed in order to investigate the effect upon the stresses developed in both the broken fiber as well as in neighboring unbroken fibers. Unlike the unit cells described above, more than one fiber per unit cell is now required. The geometry for the partially damaged unit cell is shown in Fig. 7b. Boundary conditions are the same as defined above for the fully damaged unit cells, except that the tensile boundary load is placed upon both the matrix and unbroken fibers at the front surface:

1) $u_1(0, y, z) = ur_2 = ur_3 = 0$
2) $u_2(x, W, z) = ur_1 = ur_3 = 0$
3) $u_3(x, y, 0) = 0$
4) $u_1(W, y, z) = \delta_1$
5) $u_2(x, W, z) = \delta_2$
6) $u_3(x, y, L) = \delta_3$ (all of surface except for bottom left broken fiber)

Single-fiber CFC unit cell models were constructed with fiber volume fractions of $V_f = 0.30$, 0.50, and 0.70. These different fiber volume fractions are used to demonstrate the effect of V_f on the fiber load transfer characteristic length, L_c. In each CFC unit cell, the fiber radius (R) and length (L)are the same, while the width (W) must change in order to account for the fiber volume fraction. In the RFC unit cell models, however, the fiber volume fraction is held at $V_f = 0.30$, and comparisons are made to the CFC with the same V_f only. Dimensions for each unit cell are given in Table 1.

Table 1. Unit Cell Dimensions.

Unit Cell	Type	R (μm)	L (μm)	W (μm)	V_f
UC-1	CFC single-fiber	7.0	35.0	11.325	0.30
UC-2	CFC single-fiber	7.0	35.0	8.775	0.50
UC-3	CFC single-fiber	7.0	35.0	7.415	0.70
UC-4	RFC single-fiber	3.5	35.0	5.6625	0.30
UC-5	RFC four-fiber	3.5	35.0	11.325	0.30
UC-6	RFC/CZM four-fiber	7.0	35.0	11.325	0.30
UC-7	CFC/CZM single-fiber	7.0	35.0	11.325	0.30
UC-8	RFC/CZM single-fiber	3.5	35.0	5.6625	0.30

D. Boundary Loads

An effort has been made to ensure that the reaction force in the axial direction (RF) developed at the back surface of each model is the same, thus ensuring that the *fiber* in each unit cell is under a comparable load. The loads required for each unit cell to ensure this are discussed below. It was found that for a constant fiber volume fraction, maintaining the same RF is unnecessary in order to simply determine and compare the fiber load transfer characteristic length, L_c, between CFC and RFC model. This conclusion (further discussed in the Results section), and the desire to clarify that it is a characteristic length independent of the actual load applied, is why the term "characteristic load transfer length" is used in this paper rather than the term "ineffective length." However, having

RF equal between models *is* helpful when comparing the stresses developed within the models. In the damageable models especially, ensuring that each fiber is under comparable loads is more indicative of the relative levels of damage tolerance for CFC and RFC materials.

E. Fiber and Matrix Materials

The constituent materials in this study attempt to represent the mechanical properties of lightweight fiber and flexible matrix materials. Standard values of vectran and polyethylene were used to simulate the fiber and matrix materials, respectively, with values shown in Table 2. For simplicity, fiber and matrix material models were assumed to be linear elastic and isotropic. Note that these values give a fiber/matrix modulus ratio of $E_f / E_m = 20$.

Table 2. Cohesive Properties and Parameters.

Mechanical Property	Vectran Fiber	Polyethylene Matrix
Elastic modulus, E (GPa)	80.0	4.0
Poisson's ratio, ν	0.23	0.37

IV. Cohesive Zone Modeling

In debonding and decohesion failure where the initial separation between the debonding surfaces is negligibly thin, the cohesive layer may be represented using the cohesive zone model (CZM) traction-separation relation. The finite element code Abaqus was used to build and analyze the micromechanical model. Here we have taken advantage of the general traction-separation framework provided by this code whereby cohesive mechanical behavior can be prescribed. Additionally, the cohesive behavior may be adapted in Abaqus through user-defined subroutines. At this time, we discuss only the main characteristics of the cohesive mechanical behavior and damage properties defined in terms of the traction-separation relation.

The cohesive behavior in this study was defined using 3D, 4-node, zero-thickness elements placed at the fiber-matrix interface between the elements representing the surrounding solid fiber and matrix constituent materials (see Fig. 8). The purpose for this arrangement was to study the relationship between the increase in interfacial surface area found in RFCs and the relative damage tolerance of the material as compared to CFCs.

A. CZM General Usage

The finite element CZM approach allows the simulation of damage initiation and damage evolution by using cohesive elements formulated with a traction-separation constitutive behavior. In this approach, cohesive elements are placed between continuum elements, forming an "interface" in which damage may occur and the surrounding continuum elements may separate. In the traction-separation relation, cohesive elements exhibit a response to loading which relates the nominal stresses to the nominal strains across the interface. In order to accurately simulate crack growth through a material, the CZM approach requires *a priori* knowledge of the direction of crack growth. In macro-scale simulations this is typically achieved through experimental observation. For the micromechanical simulations of this research, the cohesive elements have been placed where typical failure mechanisms have been observed in fiber-reinforced composites: debonding at the fiber-matrix interface.

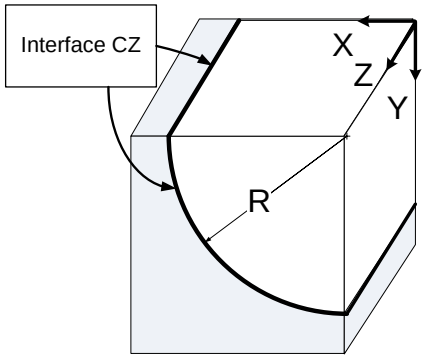

Figure 8. Placement of zero-thickness cohesive elements at fiber-matrix interface. *The bold lines indicated by the arrows show the placement of the cohesive zone (CZ).*

Multiple damage mechanisms and failure criteria have been used in the literature in order to model cohesive failure.[12-17,22,23] Often, the traction-separation behavior is defined by "tuning" the cohesive parameters in order to recreate the damage and failure mechanisms experimentally observed in real materials and material systems. The most important parameters include the damage initiation criterion (the cohesive critical strength), the cohesive energy (in CZM this is also called the work of separation, the energy dissipated due to failure, or the fracture energy G_c), and the overall shape of the traction-separation curve (including the choice of the initial cohesive element penalty stiffness, K). It is well documented in the literature that the CZM approach shows a strong mesh dependence, often related to the cohesive element edge length and the value of K.[21]

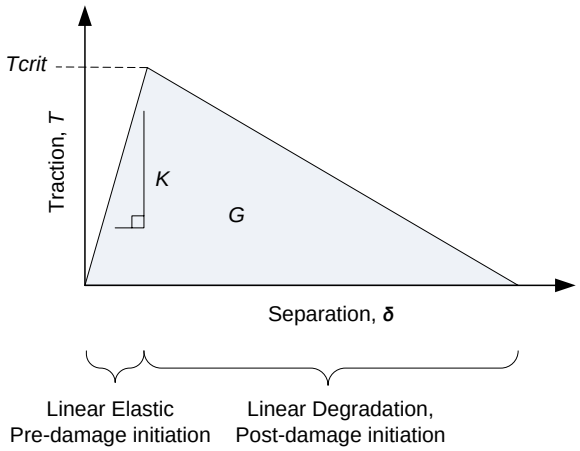

Figure 9. Bilinear traction-separation.

B. Cohesive Mechanical Behavior

Cohesive properties used in this investigation are representative of those used in the literature for glass fibers and epoxy matrices,[22] which are given in Table 3. Damage initiation is based upon a critical nominal stress criterion (T_c), damage evolution is based upon the fracture energy (G_c) criterion using the Benzeggagh-Kenane (BK) mixed-mode form,[23] and a simple bilinear shape for the traction-separation relation has been assumed.

Table 3. Cohesive Properties and Parameters.

Mechanical Property	Value
Penalty Stiffness, K (GPa)	500
Critical Nominal Stress, T_c (MPa)	25
Work of Separation, G_c (N/m)	500
BK Material Fitting Parameter, m	2.284

In the bilinear shape, a linear elastic response is assumed until the damage initiation criterion has been satisfied. If loading continues beyond this point, the response is defined by a linear degradation of element stiffness. As is shown in Fig. 9, the area under the traction-separation (T-δ) curve represents the cohesive critical fracture energy, G_c. When G_c has been satisfied, the cohesive element stiffness has reduced to zero, the element can make no further contribution to the global stiffness matrix, and has effectively "broken."

In this paper, for simplicity, cohesive values have been assumed to be the same in normal, shear, and transverse shear directions. Attempts to recreate physical experiments are not made in this paper. Rather, investigations concentrate on the potential advantages posed by increases in the interfacial surface area in composites with reduced fiber diameters. Therefore, only comparisons between conventional fiber diameters and reduced fiber diameters are discussed for these damage models.

V. Results

The analyses presented here investigated a number of unit cells to determine the stress distributions, the load transfer characteristic lengths, and the damage tolerance of RFCs relative to composites with fibers of conventional diameter (CFC). In these analyses, the shear stress developed at the fiber-matrix interface in the matrix material (τ) and the axial stress developed in the fiber center (σ) are determined. Results from these investigations are grouped into four categories:

1) CFC unit cells
2) RFC unit cells
3) Four-fiber RFC unit cell (one broken fiber, while the others are intact)
4) Damage models (CFC and RFC)

A. Conventional Fiber-Diameter Unit Cells

This section describes results from unit cells with conventional fiber diameters (UC-1, UC-2, and UC-3). First, we demonstrate that for a specified V_f the fiber load transfer characteristic length, L_c, remains unchanged even as the magnitude of loading changes. Although the change in L_C as V_f varies is often reported in the literature, to the authors' knowledge this is the first time this result has been specifically shown. Results are shown in Fig. 10 for two boundary displacements placed on UC-1 (with $V_f = 0.30$) of:

1) $u_3 = 0.2$ μm
2) $u_3 = 0.4$ μm

The length of fiber required before 90% of the maximum stress developed within in each fiber is the same in each load case, as illustrated by the dotted lines in the figure. The rate at which the axial stress within the fiber increases to its maximum is also the same, as shown in Fig. 11. Thus, the length of fiber required for stress transfer is a characteristic value for a given V_f and modulus ratio.

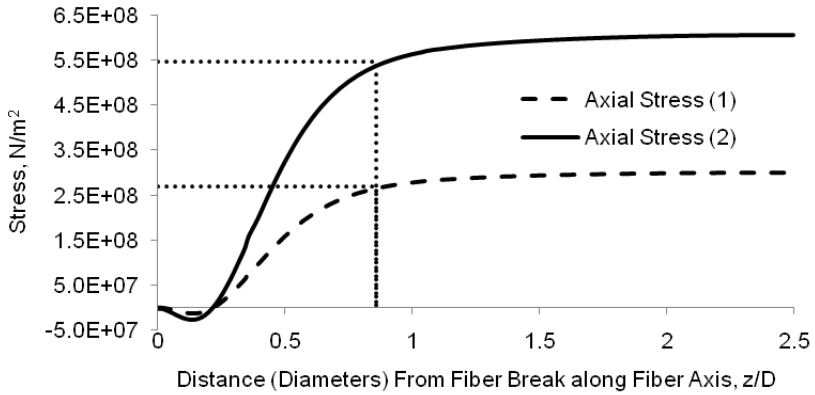

Figure 10. The 90% load transfer length for the single fiber model as a function of fiber diameter in two load cases. *For $V_f = 0.30$, the load transfer characteristic length is approximately 12.5 μm (or approximately 89% of a fiber diameter) for both load case (1) and (2).*

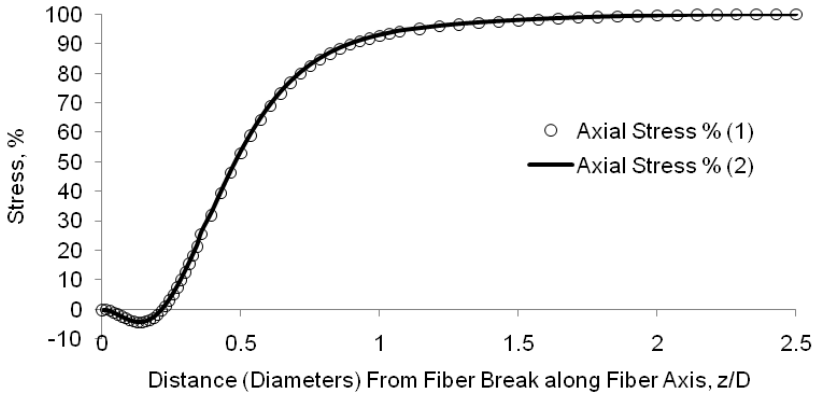

Figure 11. The percent of maximum axial stress for the single fiber model as a function of fiber diameter. *The rate at which the maximum stress in each fiber is developed is the same for load cases (1) and (2). Results are shown for $V_f = 0.30$.*

The axial stresses developed in the fibers of UC-1, UC-2 and UC-3 are compared in Fig. 12, where the boundary displacement for each unit cell has been tuned such that the reaction force, *RF*, developed at the back surface of each unit cell is constant. For clarity, this result is repeated in Fig. 13, where the fiber axial stress, σ, is normalized by the maximum stress developed in the fiber, σ_{max}. As reported by Nairn,[5] Hossain et al.,[11,18] and others, this characteristic load transfer length decreases as fiber volume fraction increases. Here it can be seen that the nondimensional value L_c occurs at nearly the same percent of the maximum load carried in the fiber; here L_c is calculated using Eq. (7),

where z_c is the length required for 90% of the maximum axial stress to be developed in the fiber, and D is the fiber diameter.

$$L_c = z_c / D \tag{7}$$

This equation, therefore, represents a ratio of length to diameter, and can be interpreted as the number of fibers required before 90% of the maximum axial load has been recovered by a broken fiber. Results are summarized in Table 3. For each CFC unit cell, the shear stresses, τ, developed at the fiber-matrix interface in relation to the axial stresses, σ, are shown in Fig. 14.

Table 3. Load Transfer Characteristic Length, L_c.

Unit Cell	Type	V_f	L_c (z_c /D)	σ/σ_{max}
UC-1	CFC single-fiber	0.30	0.89	0.91
UC-2	CFC single-fiber	0.50	0.79	0.91
UC-3	CFC single-fiber	0.70	0.71	0.90

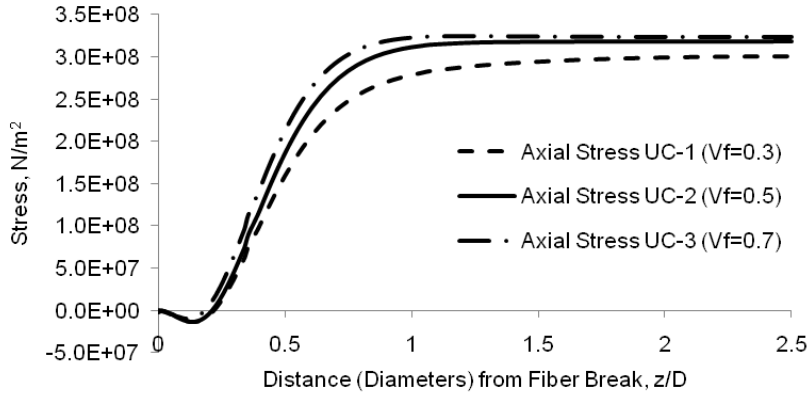

Figure 12. Axial stress developed in CFC models as a function of fiber diameter. *Results indicate the decrease in L_c as V_f increases.*

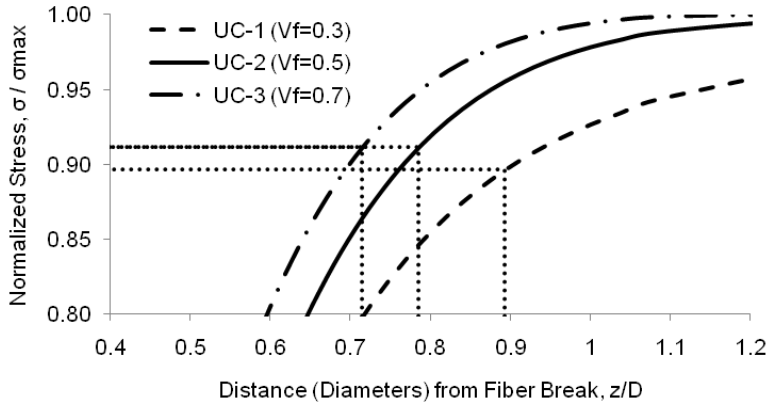

Figure 13. Zoomed view of normalized axial stress developed in CFC models as a function of fiber diameter. *Stress, σ, is normalized by the maximum σ_{max} developed in the fiber. Results indicate the decrease in L_c as V_f increases.*

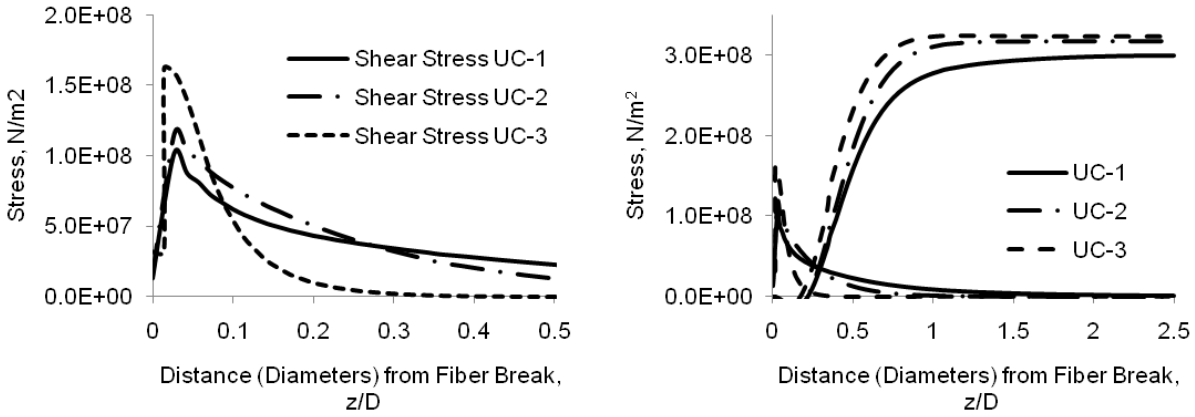

Figure 14. Zoomed views of (a) Shear stresses in each CFC unit cell, and (b) Relationship between shear and axial stresses in each CFC unit cell.

B. Reduced Fiber-Diameter Unit Cells

This section describes results from unit cells with reduced fiber diameters, UC-4 and UC-5. In UC-4 (with $V_f = 0.30$), an infinite plane of broken fibers was simulated through the use of the single-fiber model and appropriate boundary conditions (as previously described). Therefore, direct comparisons with respect to stress distributions and L_c can be made between UC-4 and UC-1. In order to compensate for the reduction in total cross-sectional area at the back surface of UC-4 (as compared to UC-1), the boundary displacement was tuned such that the resulting reaction force in the axial direction (RF) developed at the back surface was properly scaled, thus ensuring that the *fiber* in both unit cells are under a comparable load. The scaling of geometry for each unit cell is shown in Fig. 5. above. Note that the width of unit UC-1, $W_{\text{UC-1}}$, is four times the width of UC-4, $W_{\text{UC-4}}$. As such, the desired reaction force at the back surface of UC-4 is $RF_{\text{UC-4}} = 0.25RF_{\text{UC-1}}$. The geometry, displacement loads, and reaction forces for UC-1 and UC-4 are given in Table 4. The resulting stress distributions for UC-1 and UC-2 are compared in Fig. 15.

The axial stress, σ, develops much more rapidly in the RFC unit cell as compared to the CFC unit cell. Once fully developed, both fibers experience the same axial stress (indicating correct boundary conditions have been

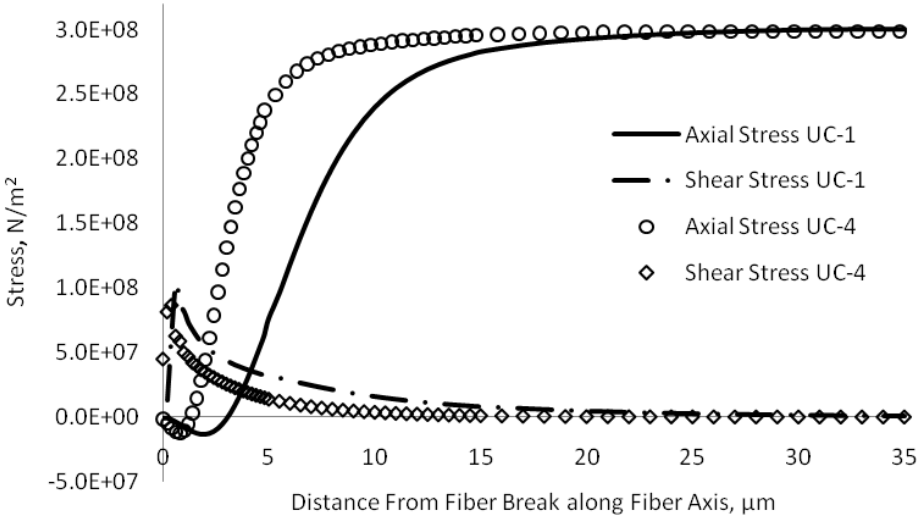

Figure 15. Shear and axial stress comparison in the CFC, UC-1, and the RFC, UC-4. *The axial stress more quickly in UC-4, while the shear stress decreases more rapidly. Results are shown for $V_f = 0.30$.*

applied). Similarly, the shear stress, τ, developed in the RFC unit cell decreases much more rapidly as compared to the CFC unit cell. These results have been further investigated in the companion to this paper.[18] The 90% fiber load transfer characteristic length, L_c, for each unit cell are shown in Table 4.

Table 4. Geometry, tensile boundary displacements, and reaction forces for UC-1 and UC-4.

Unit Cell	Type	V_f	L (μm)	R (μm)	W (μm)	δ_3 (μm)	RF (N)	L_c (z_c/D)
UC-1	CFC single-fiber	0.30	35	7.0	11.325	0.20	12.641E-3	0.89
UC-4	RFC single-fiber	0.30	35	3.5	5.6625	0.164	3.1603E-3	0.90

As shown in Eq. (8), the fiber load transfer characteristic length is normalized by the fiber diameter. The axial stress shown in Fig. 16b is plotted as a function of the normalized distance from the fiber break for each unit cell, where for UC-1we use the axis normalization *z/D*, and for UC-2 we use *z/d*. Therefore, in the normalized axis of Fig. 16b, the data points for UC-1 appear to end sooner – this is simply a result from the larger diameter *D* in the CFC (fewer fiber diameters *D* than *d* occur in the unit cell length *L*). From this figure it becomes apparent that although the axial stress in the reduced fiber-diameter composite recovers the maximum stress very rapidly, the characteristic length, L_c, is the same for both fiber diameters in the CFC of UC-1 and the RFC of UC-2. These results indicate that L_c changes only with V_f or the fiber-matrix modulus ratio, and is relatively unaffected by fiber diameter.

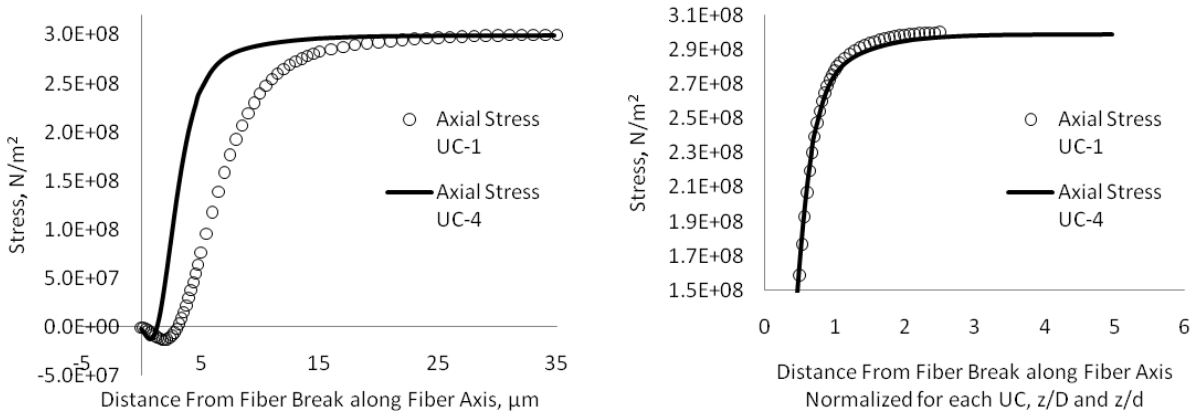

Figure 16. (a) Fiber axial stresses as a function of model length, and (b) Normalized fiber axial stresses in each CFC unit cell.

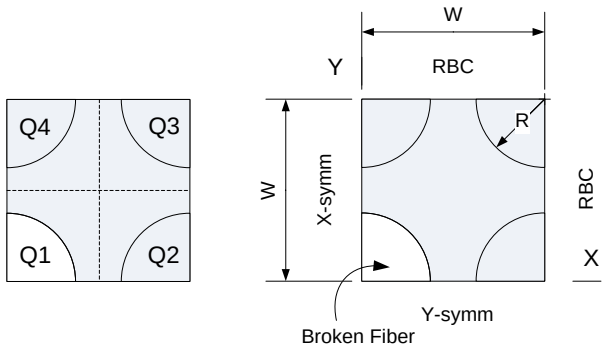

Figure 17. (a) Partially damaged unit cell with quarter designations, and (b) Partially damaged unit cell with four fibers with geometry and BCs. *Quarter designations are provided in order to present results. All loading is performed in the shaded regions only.*

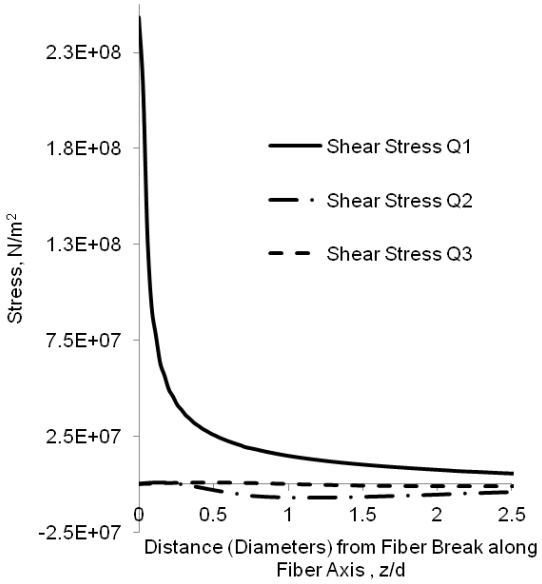

Figure 18. Shear stresses in quarter sections of UC-5. *The shear stress developed in Q1 is orders of magnitude larger than in the neighboring fibers. Results are shown for $V_f = 0.30$.*

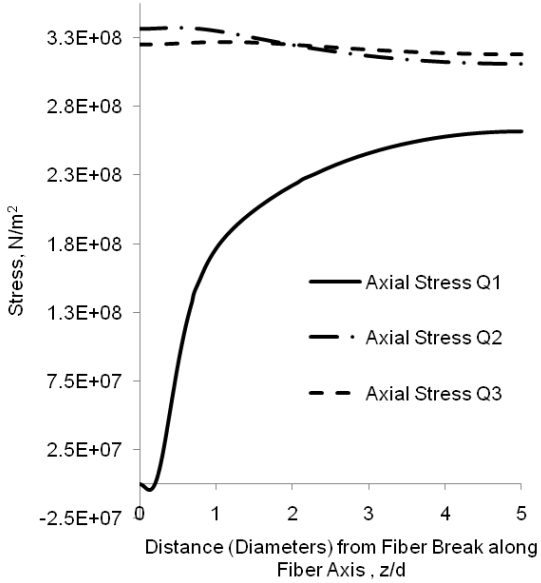

Figure 19. Axial stresses in quarter sections of UC-5. *The axial stress developed in Q1 is less than found in the neighboring fibers, increasing only very slowly once L_c has been reached. Results are shown for $V_f = 0.30$.*

C. Four-fiber Reduced Diameter Unit Cell

In UC-5, the reduced fiber-diameter composite (RFC) was also used to represent a unit cell with partial fiber damage (see Fig. 17b). In these unit cells, only one in 9 fibers are broken in the loading plane when symmetry expansion is considered. This allows an investigation into the behavior of damaged or broken fibers in the presence of neighboring unbroken fibers. Conversely, the arrangement allows an investigation into the shear-lag response of an unbroken fiber when in the vicinity of a broken fiber. In order to present the results from this model clearly, each quarter-section of the four-fiber unit cell is designated as shown in the figure (i.e., the lower left section of the unit cell is designated "Q1").

It was found that, due to the symmetry of the four-fiber model, results from Q2 and Q4 were identical. Upon consideration, it became clear that a 45° wedge of the unit cell may have been substituted with appropriate boundary conditions. Thus, to conserve space and avoid repetition results are discussed for Q1, Q2, and Q3 only. In these results, we present again the shear stress developed at the fiber-matrix interface, and the axial stress in the fiber center. Fig. 18 illustrates the shear stress response found in Q1, 2, and 3, while Fig. 19 shows the axial stress response for the same quarters. Stress results are then presented for Q1 alone in Fig. 20, the axial stresses in Q2 and Q3 in Fig. 21, and the shear stresses in Q2 and Q3 in Fig. 22.

Interestingly, these results show that for a fiber volume fraction of $V_f = 0.30$ the broken fiber does not recover a maximum axial stress equivalent to that found in the unbroken neighbor fibers within an axial distance of 5 fiber diameters from the fiber break plane, and the stress distributions of neighboring unbroken fibers are only slightly perturbed. Shear stress at the fiber-matrix interface is large at the broken fiber only, where a large amount of stress is redistributed back into the broken fiber across the fiber-matrix interface. This stress transfer redistribution coincides with the decrease in axial stress seen in the neighbor fibers.

The fiber load transfer characteristic length for the broken fiber in UC-5 was determined to be approximately $L_c = z_c / \mathrm{d} = 18\ \mu\mathrm{m} / 7\ \mu\mathrm{m} = 2.6$. This represents a large change in value from the characteristic length found in UC-4 for the same fiber diameter and volume fraction (where $L_c = 0.90$). This change is attributed to the influence of the surrounding unbroken fibers in UC-5. Indeed, it appears from the course of this research that the influence of surrounding fibers (broken or unbroken) is the primary factor affecting the fiber load transfer characteristic length of a broken fiber.

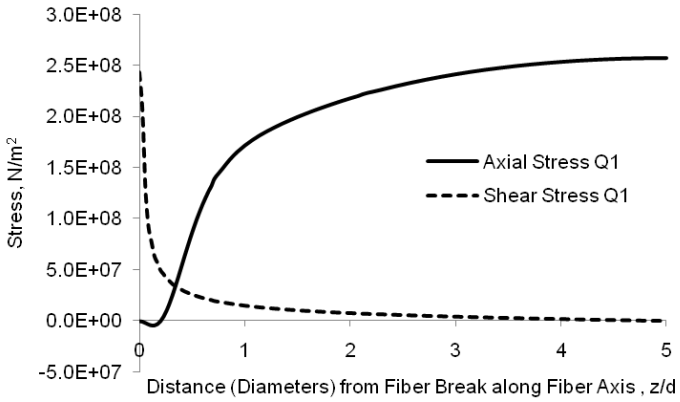

Figure 20. Shear and axial stress in Q1 (broken fiber).

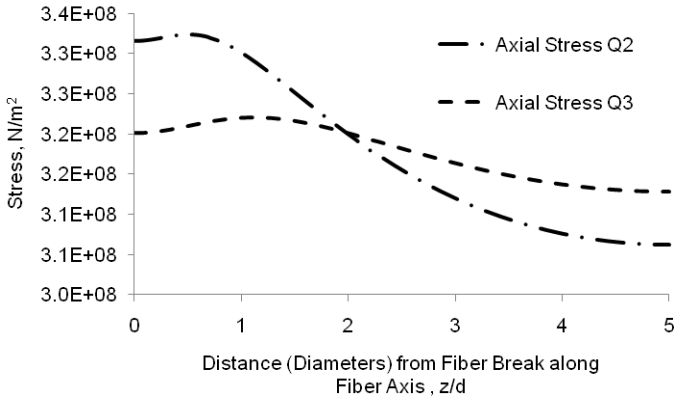

Figure 21. Axial stress in Q2 and Q3 (unbroken fibers).

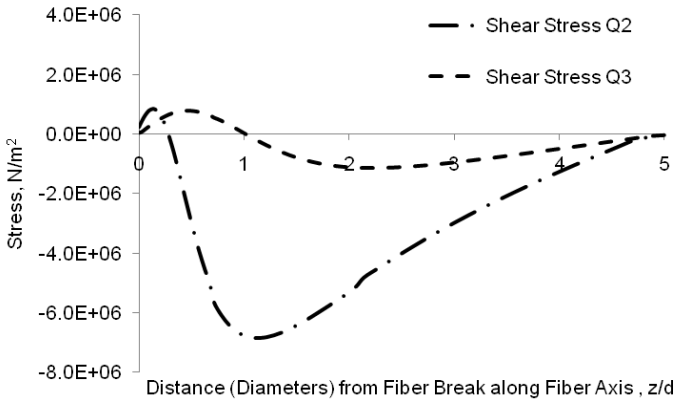

Figure 22. Shear stress in Q2 and Q3 (unbroken fibers).

D. Unit Cells with Cohesive Damage

The final results presented here include data from the CFC unit cell UC-1 and the RFC unit cell UC-4, where a damageable layer of cohesive elements were placed at the fiber-matrix interface. Thus, these unit cells are renamed UC-7 and UC-8, respectively, in order to help in their identification. In all other respects, such as the geometry and boundary constraints, these models are the same as their parent models. These unit cells are appropriate for comparing the response of a broken fiber and its characteristic load transfer length between CFC and RFC models,

and are consistent with standard shear-lag theory models. The cohesive zone models can also represent the important composite material failure modes of fiber-matrix debonding and fiber pull-out; however, the main goal in the current investigation is to simply qualitatively recognize the potential differences in damage resistance between CFC and RFC models. Typical glass-epoxy cohesive parameters are used (as given above in Table 3). Unit cell information is given in Table 5.

Table 5. Geometry, tensile boundary displacements, and reaction forces for UC-1 and UC-4.

Unit Cell	Type	V_f	L (μm)	R (μm)	W (μm)	δ_3 (μm)	RF (N)	L_c (z_c/D)
UC-7	CFC single-fiber	0.30	35	7.0	11.325	0.020	1.230E-3	0.89
UC-8	RFC single-fiber	0.30	35	3.5	5.6625	1.16E-2	0.307E-3	0.93

The resulting shear and axial stress distributions for the CFC model (UC-7) and for the RFC model (UC-8) are presented below. Effort has been undertaken in order to maintain a constant reaction force developed in the axial direction at the back surface of both models. Here again, notice that due to unit cell scaling for the RFC (in order to maintain the fiber volume fraction) 1/4 of the reaction force found in UC-7 is desired in UC-8. The load transfer characteristic length is determined from the results shown in the figures below.

In Fig. 23, the axial and shear stress distribution in UC-7 and UC-8 are shown where the horizontal axis has been normalized by fiber diameter. The axial stress results are plotted separately in Fig. 24, where the horizontal has not been normalized, and is the *z*-distance from the plane of the fiber break along the fiber axis. Shear stress results are also plotted separately in Fig. 25 also against the *z*-distance for the first 15 μm from the plane of the fiber break.

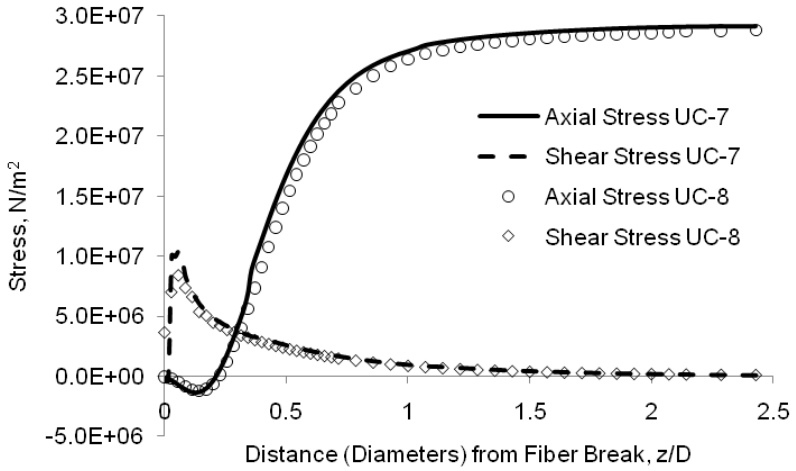

Figure 23. Stress distribution in UC-7 and UC-8.

From Fig. 23, we can see that L_c is quite similar between the RFC and CFC unit cell models. It can also be seen from Fig. 24 that the axial stress in the RFC model increases towards σ_{max} more quickly than in the CFC model (as was seen for the non-CZM models). As in previous results, the maximum shear stress τ_{max} is lower in the RFC model, and decreases more quickly.

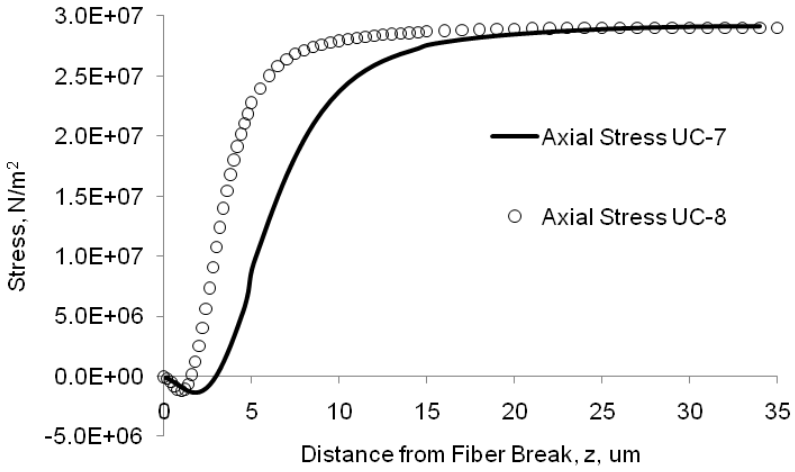

Figure 24. Axial stress (σ) distribution in UC-7 and UC-8.

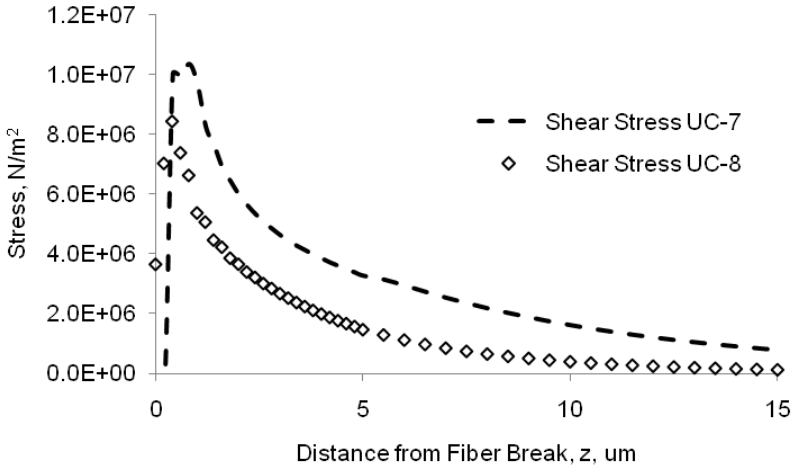

Figure 25. Axial stress (σ) distribution in UC-7 and UC-8.

Note that for the loading condition specified in these models, the first row of elements in the cohesive zone next to the fiber break have satisfied the damage initiation criterion (the quadratic stress criterion) as shown below. In this formulation, an undamaged element has a value of zero, and damage initiates when the criterion reaches a value of 1.0. As briefly described above, once the damage criterion has been satisfied, a cohesive element exhibits a reduction in stiffness until it offers no further resistance to loads.The damage initiation criterion was monitored in four locations along the length of the fiber in the cohesive zone at the fiber-matrix interface during the load step. Values reported in the following figures indicate the change in the damage initiation criterion over the FE step-increment time.

As indicated in the figures, the damage initiation criterion is satisfied in UC-7 at a distance of $z = 0$ μm from the fiber break plane, whereas by the end of the load step at the same location UC-8 accumulates approximately 20% the inititation criterion. The value for the damage initiation criterion in the RFC unit cell is significantly less than that in the CFC unit cell for each location along the cohesive fiber-matrix interfacial region, except for at $z = 2$ μm (illustrated by Fig. 26). At $z = 2$μm the trend is reversed, and in fact UC-8 indicates a higher criterion.

From these results, it is proposed that the reduced fiber-diameter composite materials will experience less damage and greater damage tolerance as compared to the conventional fiber-diameter composites. The locations where the damage initiation criterion were monitored and the final damage initiation criterion value at the end of the load step are given in Table 6. In Fig. 27 the damage initation criterion in UC-7 and UC-8 are compared for the final FE-time increment only.

Table 6. Damage Inititation Criterion at four locations along fiber axis for UC-7 and UC-8.

Unit Cell	Type	V_f	z = 0 μm	z = 2 μm	z = 5 μm	z = 15 μm
UC-7	CFC single-fiber	0.30	1.0	0.0073	0.0194	0.0011
UC-8	RFC single-fiber	0.30	0.2610	0.1928	0.0061	4.4E-05

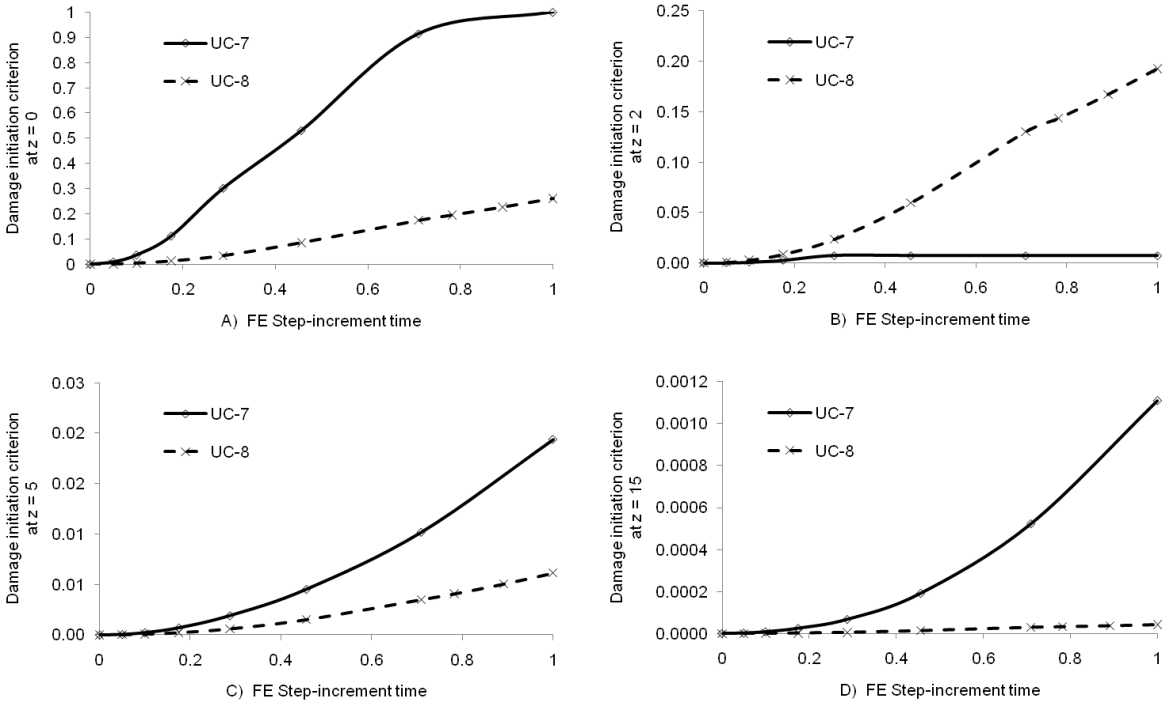

Figure 26. Damage initiation criterion in UC-7 and UC-8.

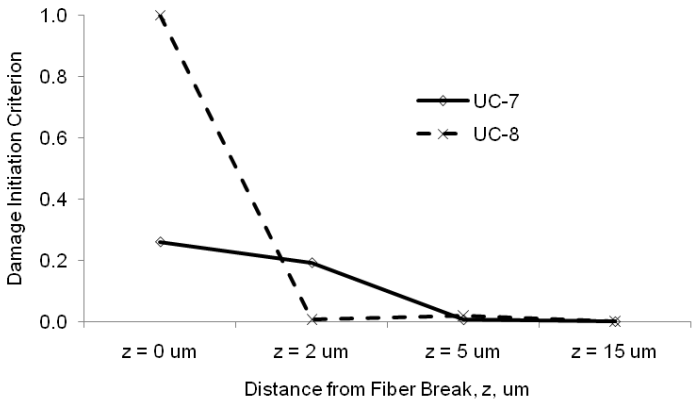

Figure 27. Damage Initiation Criterion values in UC-7 and UC-8 at the final FE Step-increment in cohesive elements at fiber-matrix interface, along the fiber length.

VI. Conclusion

The effect of reducing the fiber diameter upon the durability and damage tolerance of thin flexible composites in unidirectional fiber reinforced flexible-matrix composites was investigated through the current research. This work has indicated that damage tolerance in composites with conventional fiber diameters (CFC) may improved by reducing the fiber diameters, while keeping the fiber volume fraction, V_f, constant. Finite element shear-lag analysis shows that the 90% fiber stress transfer length is significantly reduced in composites with reduced fiber diameters (RFC). However, it is also shown herein that the nondimensional fiber load transfer characteristic length, L_c, remains constant when V_f is held constant as the fiber diameter is reduced. The work presented here has also demonstrated that the fiber load transfer characteristic length, L_c, remains constant for a given V_f as the magnitude of the load condition changes.

Useful work that may be performed in the future include experimental validation of the relative damage tolerance between reduced fiber-diameter and conventional fiber-diameter composites. Numerical investigations would be improved when considering fiber-reinforced composite damage tolerance levels when local variations in the fiber-matrix bond quality are also accounted for and present in the model. The presence of interphase properties often detected at fiber-matrix interfaces were neglected in this paper. The results included in this paper also neglected, but would be enhanced by, including the residual stresses common to most glass-epoxy composites resulting from manufacturing and mismatches in CTE in the fiber and matrix.

References

[1]Jenkins, C.H.M. (ed.), *Gossamer Spacecraft: Membrane and Inflatable Structures Technology for Space Applications*, Progress in Astronautics and Aeronautics, Vol. 191, AIAA, 2001, pp. 2, 243-254.

[2]Aboudi, J., "Micromechanical Analysis of Composites by the Method of Cells," *ASME*, 1989.

[3]Aboudi, J., "Micromechanics Prediction of Fatigue Failure of Composite Materials," *Journal of Reinforced Plastic Composites*, 1989.

[4]Cox, H.L., "The Elasticity and Strength of Paper and Other Fibrous Materials," *British Journal of Applied Physics*, 3, 72.

[5]Nairn, J.A., "On the Use of Shear-Lag Methods for Analysis of Stress Transfer in Unidirectional Composites," *Mechanics of Materials*, No. 26, 1996, pp. 63-80.

[6]Goh, K.L., Aspden, R.M., Hukins, D.W.L., Shear lag models for stress transfer from an elastic matrix to a fiber in a composite material, *Int. J. Materials and Structural Integrity*, Vol. I, Nos. 1/2/3, 2007.

[7]Chon, C. T., & Sun, C. (1980). Stress distributions along a short fiber in fiber reinforced plastics. 15, 931-938.

[8]Xia, Z., Okabe, T., & Curtin, W. (2002). Shear-lag versus finite element models for stress transfer in fiber-reinforced composites. *Composites Science and Technology*. Vol. 62, 1141-1149.

[9]Li, H., Jia, Y., Mamtimin, G., Jiang, W., An, L., "Stress transfer and damage evolution simulations of fiber-reinforced polymer-matrix composites," *Materials Science and Engineering A*, No. 425, 2006, pp. 178-184.

[10]Milliren, E.C., Nanocomposites: A Study of Theoretical Micromechanical Behavior Using Finite Element Analysis, *Graduate Thesis, Department of Mechanical and Industrial Engineering, Montana State University, Bozeman, Montana59717.*

[11]Hossain, N.M., Milliren, E.C., Woo, K. and Jenkins, C.H. (2010), "The Effect of Fiber Diameter on the Strength of Lightweight Composites," *51st AIAA/ASME/ASCE/AHS Structures, Structural Dynamics, and Material Conference*, Orlando, Florida.

[12]Barenblatt, G.I., "The mathematical theory of equilibrium cracks in brittle fracture," *Advances in Applied Mechanics*, Vol. 7, 1962, pp. 55-129.

[13]Dugdale, D.S., "Yielding of steel sheets containing slits," *Journal of the Mechanics and Physics of Solids*, Vol. 8, 1960, pp. 100-104.

[14]Needleman, A., "An analysis of decohesion along an imperfect interface," *International Journal of Fracture*, Vol. 42, 1990, pp. 21-40.

[15]Tvergaard, V., "Effect of pure mode I, II or II loading or mode mixity on crack growth in a homogeneous solid," *International Journal of Solids and Structures*, Vol. 47, 2010, pp. 1611-1617.

[16]Camanho, P.P., and C.G. Davila, "Mixed-Mode Decohesion Finite Elements for the Simulation of Delamination in Composite Materials," NASA/TM-2002–211737, pp. 1–37, 2002.

[17]Chandra, N., Li, H., Shet, C., and Ghonem, H., "Some issues in the application of cohesive zone models for metal-ceramic interfaces," *International Journal of Solids and Structures*, Vol. 39, 2002, pp. 2827-2855.

[18]Hossain, N.M., Peterson, W.M., Woo, K. and Jenkins, C.H. (2011), "Strength of flexible composites: Effect of fiber scaling," *52st AIAA/ASME/ASCE/AHS Structures, Structural Dynamics, and Material Conference*, Denver, Colorado (to be published).

[19]Kaw, A. K., *Mechanics of Composite Materials*, 2nd ed., CRC Press, Boca Raton, 2006, Chap. 1.

[20]Kanit, T., Forest, S., Galliet, I., Mounoury, V., Jeulin, D., "Determination of the size of the representative volume element for random composites: statistical and numerical approach." *International Journal of Solids and Structures*, Vol. 40, 2003, 3647-3679.

[21]Turon, A., Davila, C.G., Camanho, P.P., Costa, J., "An engineering solution for mesh size effects in the simulation of delamination using cohesive zone models," *Engineering Fracture Mechanics*, Vol. 74, 2007, pp. 1165-1682.

[22]Alfaro, M.V. Cid, Suiker, A.S.J., De Borst, R., “Transverse failure behavior of fiber-epoxy systems.” *Journal of Composite Materials*, Vol. 44, No. 12, 2010, pp. 1493-1516.
[23]Benzeggagh, M.L., Kenane, M., "Measurement of mixed-mode delamination fracture toughness of unidirectional glass/epoxy composites with mixed-mode bending apparatus," *Composites Science and Technology*, Vol. 56, 1996, 439-449.